SIAM J. NUMER. ANAL.
Vol. 54, No. 3, pp. 1899–1919




# ASYMPTOTICALLY COMPATIBLE FOURIER SPECTRAL APPROXIMATIONS OF NONLOCAL ALLEN–CAHN EQUATIONS*

QIANG DU† AND JIANG YANG†

**Abstract.** We study Fourier spectral approximations of a nonlocal Allen–Cahn (NAC) equation that reduces to the conventional Allen–Cahn equation in the local limit. We show that the Fourier spectral methods are asymptotically compatible in the sense that they provide convergent approximations to both nonlocal and local models. Furthermore, we provide various error estimates. In particular, it is shown that the numerical solutions of nonlocal models converge to those of the corresponding local models uniformly at a rate of $O(\delta^2)$. This is achieved by first establishing a similar result for linear nonlocal diffusion equations. A careful investigation, both analytically and computationally, is made of the steady state solutions of NAC equations, demonstrating how discontinuities may appear in solutions and how they are related to model parameters.

**Key words.** asymptotically compatible schemes, nonlocal models, Fourier spectral methods, nonlocal Allen–Cahn equations, error estimates

**AMS subject classifications.** 65M70, 65R20

**DOI.** 10.1137/15M1039857

## 1. Introduction.

This work is concerned with the numerical solution of some nonlinear nonlocal models and their local limit. We supplement both nonlocal and local models with periodic boundary conditions so that it is natural to consider Fourier spectral methods. We focus on an illustrative model problem associated with a nonlocal Allen–Cahn (NAC) equation that is a nonlocal analogue of the conventional, local Allen–Cahn (LAC) equation [2]. The NAC can be obtained by replacing the standard diffusion operator in the LAC with a nonlocal diffusion operator $\mathcal{L}_\delta$, defined by

$$\mathcal{L}_\delta u(x) = \int_{|s|\le\delta} \rho_\delta(s)\,(u(x+s)-u(x))\,ds, \tag{1.1}$$

where $\delta$ is called a horizon parameter and the kernel $\rho_\delta = \rho_\delta(s)$ is a nonnegative, radial function (i.e., $\rho_\delta(s) = \rho_\delta(|s|)$ for any $s$), compactly supported in $|s| \le \delta$, and has a bounded second moment [3, 16, 17].

In recent years, many studies of nonlocal models have appeared in various applications in physics, biology, materials science, and social science, for instance, phase transitions [6, 22], nonlocal heat conduction [7], nonlocal Dirichlet forms [4], kinetic equations [27], and image analyses [9, 23, 28]. To account for nonlocal spatial interactions, a nonlocal model often takes the form of an integral equation that avoids the explicit use of spatial derivatives. The resulting model may thus allow its solution to develop spatial singularities that can be used to characterize the effect of various types of heterogeneities and defects. An illustrative example is the nonlocal peridynamics (PD) continuum theory introduced in [36], which has been used to study cracks and materials failure [5, 30, 38, 39]. Meanwhile, one can also find a great deal of rigorous

*Received by the editors September 15, 2015; accepted for publication (in revised form) March 15, 2016; published electronically June 23, 2016. This research was supported in part by NSF grant DMS-1318586, AFOSR MURI Center for Material Failure Prediction through Peridynamics, and ARO MURI grant W911NF-15-1-0562.

http://www.siam.org/journals/sinum/54-3/M103985.html

†Department of Applied Physics and Applied Mathematics, Columbia University, New York, NY 10027 (qd2125@columbia.edu, jy2759@columbia.edu).

mathematical analysis of nonlocal models [1, 3, 12, 20]. In [16, 17], an attempt is made to develop a more systematic mathematical framework for nonlocal problems, in parallel to that for local classical partial differential equations (PDEs). As exact solutions of nonlocal models are generally not readily available, numerical methods play important roles in the study of these models [8, 14, 18, 29, 34, 37, 44, 46].

The horizon parameter $\delta$ is often used to measure the range of nonlocal interactions in many nonlocal models. For suitably defined kernels, as $\delta \to 0$, only the effect of local interactions remains so that the zero-horizon (thus local) limit of the nonlocal operator defined in (1.1) becomes the local differential operator (second-order derivative $\partial_x^2$ in one dimension), which is denoted as $\mathcal{L}_0$ here for convenience. A discretization scheme that preserves such limiting behavior is called an asymptotically compatible scheme, a notion developed in [42, 43]. A general abstract mathematical framework was developed in [43] for the rigorous numerical analysis with respect to the Galerkin approximations of certain classes of parametrized linear problems and their asymptotic limit. In the nonlocal setting, the $\delta \to 0$ limit process provides both connection and consistency between nonlocal and local models and has practical significance, especially for multiscale modeling and simulations.

A major objective of our work is to show that Fourier spectral methods are asymptotically compatible for nonlinear NAC models associated with suitable kernels and can preserve the limiting behavior at the discrete level. Mathematically, this may be formulated as

$$(\mathrm{P}_0) = \|u_N^\delta - u^0\|_2 \to 0 \quad \text{as} \quad \delta \to 0,\ N \to \infty. \tag{1.2}$$

Moreover, we would like to provide a priori error estimates with respect to parameters $\delta$ and $N$. The desired results may be obtained through different means. For example, we may attempt to derive them by either of the following two different triangle inequalities:

$$\|u_N^\delta - u^0\|_2 \le \|u_N^\delta - u_N^0\|_2 + \|u_N^0 - u^0\|_2 = (\mathrm{P}_{1,1}) + (\mathrm{P}_{1,2}), \tag{1.3}$$

$$\|u_N^\delta - u^0\|_2 \le \|u_N^\delta - u^\delta\|_2 + \|u^\delta - u^0\|_2 = (\mathrm{P}_{2,1}) + (\mathrm{P}_{2,2}). \tag{1.4}$$

Here $u^\delta$ and $u^0$ are exact solutions to nonlocal models and their local limit, respectively. Correspondingly, $u_N^\delta$ and $u_N^0$ are numerical approximations. As a visual illustration, following [43], we put all of these inequalities in a diagram in Figure 1.

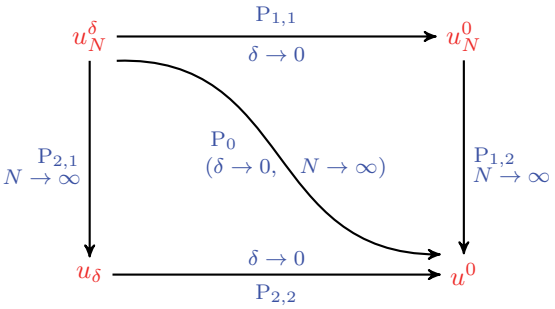


FIG. 1. *Convergence paths from* $u_N^\delta$ *to* $u^0$.

In this work, we adopt (1.3) rather than (1.4). This preference is based on two reasons. First, if we attempt to follow the path implied by (1.4) and estimate $\mathrm{P}_{2,1}$ (the

error of the spectral approximation of nonlocal models), then high regularity assumptions on $u^\delta$ are often required. However, in many cases such high regularity cannot always be guaranteed, because the existence of singular (discontinuous) solutions is often considered an advantage of nonlocal models to better capture the singularities of physical solutions. Second, even if one can prove the convergence of numerical approximations of nonlocal models with respect to a fixed horizon parameter $\delta$, the convergence behavior may be dependent on $\delta$. On the other hand, in order to follow (1.3), it simply remains to work out $\mathrm{P}_{1,1}$, which is a focus of this work, given that $\mathrm{P}_{1,2}$ has been extensively studied for the classical LAC, a well-known phase-field type equation [2]. In the literature, LAC is also called the nonlinear Ginzburg–Landau equation following the work of Landau on phase transformations. It should be pointed out that there have been many studies done on various numerical approximations and fractional order extensions of LAC, including the use of Fourier spectral approximations; see, for example, [10, 13, 19, 21, 25, 31, 45] and the references therein. In [6], the existence and stability of stationary NAC models with integrable kernels in unbounded domain are studied, and it is shown that there exist stationary solutions having discontinuities across arbitrarily prescribed interfaces. The paper [24] focuses on the energy stability and convergence analysis for the NAC and Cahn–Hilliard equations with a fixed integrable kernel function for fully discrete schemes. In our work, we study Fourier spectral approximations to NAC equations given by

$$\frac{\partial u^\delta}{\partial t} = \epsilon^2 \mathcal{L}_\delta u^\delta + u^\delta - (u^\delta)^3, \tag{1.5}$$

with periodic boundary conditions. We note that the discussion on nonlocal interactions depicted in (1.5) may be traced back to the work of van der Waals (see Rowlinson [33]). Here, we use the parameter $\epsilon$ to characterize an interaction length, which is a small positive constant. The usual differential equation form of the LAC can be derived from the nonlocal model via the so-called Landau expansion [26, 32]. By deriving estimates on $\mathrm{P}_{1,1}$, we then achieve one of the main findings of this work, that is, to show that Fourier spectral methods are asymptotically compatible for both stationary and time-dependent NAC equations, with a class of nonnegative nonincreasing radial-type kernels compactly supported over $[0, \delta]$ and having a bounded second moment. Such a finding implies that the notion of asymptotic compatibility can be established for both linear variational problems, as in [43], and nonlinear variational and time-dependent problems as demonstrated here. Moreover, we observe that the results given in [43] do not readily yield a uniform error estimate of the approximations of nonlocal problems (with respect to $\delta$). In contrast, for Fourier spectral methods, we can establish a uniform error estimate for $\|u_N^\delta - u_N^0\|_2$ on the order of $O(\delta^2)$, that is,

$$\|u_N^\delta - u_N^0\|_2 \le C\delta^2 \tag{1.6}$$

for a constant $C$ independent on $N$ as $N \to \infty$. Together with existing results on the convergence of Fourier spectral methods for classical local differential equations, we can get the limiting behavior of $u_N^\delta$ in the sense of

$$\|u_N^\delta - u^0\|_2 \le C\{\delta^2 + N^{-2}\} \quad \text{or} \quad \|u_N^\delta - u^0\|_2 \le C\{\delta^2 + e^{-cN}\}$$

for some generic constant $c$ depending on the regularity of exact solutions to local models. In our analysis here, the estimate (1.6) is shown first for a linear nonlocal diffusion model. This is not only a new result by itself but also a useful step for showing similar estimates for nonlinear NAC.

Besides studying the asymptotic compatibility of Fourier spectral approximations to the NAC, another main contribution of this work is to study, both numerically and theoretically, steady states of NAC equations with the following typical power law kernels with a finite horizon parameter:

$$\rho_\delta(s) = \frac{c_\alpha}{\delta^{3-\alpha}|s|^\alpha}, \quad s \in [-\delta, 0) \cup (0, \delta], \quad \alpha \in [0, 3). \tag{1.7}$$

For integrable kernels including $0 \le \alpha < 1$, we demonstrate the discontinuity formation in the steady state of NAC. We also note that there has been much interest in the discontinuous solutions for the NAC. For example, in [15] it was shown that there exist discontinuous stationary solutions of NAC equations associated with integrable kernels in the whole space. The results of our theoretical analysis and computational experiments provide further characterizations of such solutions. In particular, we show that the magnitude of discontinuities can be quantified by three parameters. Thus, we can control the discontinuities to characterize the sharp interface. To some degree, this supports the notion that nonlocal models may be effective tools for modeling interface problems because they can deal with solutions that need not be overly smoothed versions of the sharp interface. It is reminiscent of the objectives of PD-type models of elasticity and fracture mechanics [36] developed for handling cracks and damages in materials.

The rest of this paper is organized as follows. We first establish the asymptotic compatibility of Fourier spectral methods and regularity results for linear nonlocal diffusion problems in section 2. In section 3, analogous asymptotic compatibility is proved for nonlinear time-dependent NAC. Section 4 is devoted to studies of solutions of NAC via both numerical simulations and theoretical analysis. Concluding remarks are given in section 5.

**2. Preliminaries and stationary linear problems.** To better illustrate our main idea, we focus on problems defined on a one-dimensional (1D) domain $[-\pi, \pi]$ with a periodic boundary condition, and we note that the results remain valid for two- and three-dimensional (2D and 3D) cases.

**2.1. Nonlocal diffusion operator $\mathcal{L}_\delta$.** For the nonlocal operator given in (1.1), we consider the radial-type kernels

$$\rho_\delta(s) = \frac{1}{\delta^3}\rho\left(\frac{|s|}{\delta}\right) \quad \forall s \in [-\delta, \delta], \tag{2.1}$$

where $\rho = \rho(\xi)$ is a nonnegative nonincreasing function with a compact support in $[0, 1]$ and a bounded second moment, i.e.,

$$\int_0^1 \rho(\xi)\xi^2 d\xi = 1. \tag{2.2}$$

For any nonzero integer $n$, $e^{inx}$ is an eigenfunction of $\mathcal{L}_\delta$ and $\mathcal{L}_0$ under periodic boundary conditions, with the corresponding eigenvalues given, respectively, by

$$\lambda_\delta(n) = 2\int_0^\delta \rho_\delta(s)(\cos(ns) - 1)ds, \quad \lambda_0(n) = -n^2. \tag{2.3}$$

Hence, for any

$$u_N(x) = \sum_{|n|\le N} \hat{u}_n e^{inx} \in \hat{B}_N = \text{span}\{e^{inx}\}_{|n|\le N},$$

we have

$$\mathcal{L}_\delta u_N = \sum_{|n|\le N} \lambda_\delta(n)\hat{u}_n e^{inx} \quad \text{for } \delta \ge 0.$$

Let $(\cdot,\cdot)$ denote the standard $L^2(-\pi,\pi)$ inner product. Then for any $u_N$ and $v_N \in \hat{B}_N$,

$$(\mathcal{L}_\delta u_N, v_N) = (u_N, \mathcal{L}_\delta v_N) \quad \text{for } \delta \ge 0.$$

Since both $\lambda_\delta(n)$ and $\lambda_0(n)$ are strictly negative and real, we also have

$$(\mathcal{L}_\delta u_N, u_N) \le 0 \quad \text{for } \delta \ge 0.$$

Let $\hat{B}_N^o = \text{span}\{e^{inx},\ |n| \le N,\ n \ne 0\}$; i.e., $\hat{B}_N^o$ contains functions in $\hat{B}_N$ with mean zero. Then $\mathcal{L}_\delta u_N, \mathcal{L}_0 u_N \in \hat{B}_N^o$, and we have

$$\mathcal{L}_\delta^{-1} u_N^o(x) = \sum_{n\ne 0}^{|n|\le N} \frac{1}{\lambda_\delta(n)} \hat{u}_n^o e^{inx} \ \text{ for } \delta \ge 0, \ \ u_N^o(x) = \sum_{n\ne 0}^{|n|\le N} \hat{u}_n^o e^{inx} \in \hat{B}_N^o\,. \tag{2.4}$$

In this work, we focus on the Fourier spectral approximation of (1.5). We seek the approximate solution $u_N \in \hat{B}_N$ (or, more precisely, $\hat{B}_N^o$) such that the residual of the equation, when evaluated at $u_N$, is orthogonal to $\hat{B}_N$. We use $P_N$ to denote the standard spectral Fourier projection onto $\hat{B}_N$ of an element in $L^1[-\pi,\pi]$. Without ambiguity, the same notation is applied when $\hat{B}_N^o$ is used.

**2.2. Stationary linear problems.** We first study, for $f = f(x) \in L^2_{per}[-\pi,\pi]$ (periodic functions in $L^2$), the stationary linear nonlocal problem

$$-\mathcal{L}_\delta u_\delta(x) = f(x) \quad \forall x \in (-\pi,\pi) \tag{2.5}$$

and the local problem

$$-\mathcal{L}_0 u_0(x) = f(x) \quad \forall x \in (-\pi,\pi), \tag{2.6}$$

with periodic boundary conditions for both of them. The results are useful in the later study of nonlinear NAC.

We always assume a zero-mean compatibility condition on $f$ and enforce

$$\int_0^{2\pi} u_\delta(x)dx = C_0 \quad \text{for } \delta \ge 0, \tag{2.7}$$

with a given constant $C_0$ (for steady state problems, $C_0 = 0$ is often chosen). We take Fourier spectral methods to solve these two models numerically. For more background material on the Fourier spectral methods, see [35]. The numerical solutions, denoted by

$$u_N^\delta(x) = \sum_{|n|\le N} a_n^\delta e^{inx} \quad \text{and} \quad u_N^0(x) = \sum_{|n|\le N} a_n^0 e^{inx},$$

respectively, satisfy

$$-\mathcal{L}_\delta u_N^\delta = P_N[f] \quad \text{for } \delta \ge 0. \tag{2.8}$$

For simplicity, we denote $f_N = P_N[f] \in \hat{B}_N^o$; then $a_0^\delta = a_0^0 = 2\pi/C_0$. By notation introduced in (2.4), $u_N^\delta = -(a_0^\delta + \mathcal{L}_\delta^{-1} f_N)$ and $u_N^0 = -(a_0^0 + \mathcal{L}_0^{-1} f_N)$, respectively. Consequently,

$$u_N^\delta - u_N^0 = (\mathcal{L}_\delta^{-1} - \mathcal{L}_0^{-1}) f_N. \tag{2.9}$$

Our first key result is the uniform error estimate between discrete solutions of nonlocal problems and the local limit that establishes the link $P_{1,1}$ shown in Figure 1 for linear problems.

LEMMA 1 (uniform error estimate and asymptotic compatibility of Fourier spectral approximations to linear problems). *Assume that $u_N^\delta(x)$ and $u_N^0(x)$ are the numerical solutions to* (2.5) *and* (2.6)*, respectively. We have*

$$\|u_N^\delta - u_N^0\|_2 \le C\delta^2 \|f_N\|_2, \tag{2.10}$$

*where $C$ is a generic constant independent of $\delta$ and $N$.*

*Proof.* By (2.9), we have

$$\|u_N^\delta - u_N^0\|_2^2 = \sum_{n\neq 0}^{|n|\le N} \left| \frac{1}{\lambda_\delta(n)} - \frac{1}{\lambda_0(n)} \right|^2 |\hat{f}_n|^2. \tag{2.11}$$

It suffices to complete the proof by proving that

$$\frac{1}{\delta^2}\left| \frac{1}{\lambda_\delta(n)} - \frac{1}{\lambda_0(n)} \right| := S_n \le C \quad \forall |n| \ge 1. \tag{2.12}$$

Note that by the moment condition (2.2) and $1-\cos(n\delta\theta) \le n^2\delta^2\theta^2/2$, we get

$$0 \le \delta^2 |\lambda_\delta(n)| = 2\int_0^1 \rho(\theta)\,(1-\cos(n\delta\theta))d\theta \le n^2\delta^2. \tag{2.13}$$

Since $\theta^2/2 - \theta^4/24 \le 1-\cos(\theta)$, for any $\theta \in R$, we get $n^2\delta^2 - n^4/12\delta^4 \le \delta^2\lambda_\delta(n)$. Hence, when $n\delta \le \pi$, we see that

$$S_n = \frac{1}{\delta^2|\lambda_\delta(n)|} - \frac{1}{n^2\delta^2} \le \frac{1}{n^2\delta^2 - \frac{1}{12}n^4\delta^4} - \frac{1}{n^2\delta^2} \le \frac{1}{12-\pi^2}\,. \tag{2.14}$$

On the other hand, for $n\delta > \pi$, we utilize the nonincreasing property of $\rho$ to get

$$\begin{aligned} \int_0^1 \rho(\theta)\cos(n\delta\theta)d\theta &\le \int_0^{\frac{\pi}{2n\delta}} \rho(\theta)\cos(n\delta\theta)d\theta \\ &\le \int_0^{\frac{\pi}{2n\delta}} \rho(\theta)\cos(\theta)d\theta \\ &\le \int_0^{\frac{1}{2}} \rho(\theta)\cos(\theta)d\theta. \end{aligned} \tag{2.15}$$

Consequently,

$$\delta^2|\lambda_\delta(n)| \ge 2\left(\int_0^{\frac{1}{2}} \rho(\theta)(1-\cos(\theta)\right)d\theta + \int_{\frac{1}{2}}^1 \rho(\theta)d\theta) \ge C_1 > 0.$$

Here $C_1$ is a constant, independent of $\rho$ if (2.2) holds, and $\rho$ is nonnegative and nonincreasing. Thus, for the case $n\delta > \pi$, we have

$$S_n = \frac{1}{\delta^2\lambda_\delta(n)} - \frac{1}{n^2\delta^2} \le \frac{1}{\delta^2\lambda_\delta(n)} \le \frac{1}{C_1}. \tag{2.16}$$

Denoting $C = \max\{1/C_1, 1/(12-\pi^2)\}$, we get the desired claim (2.12). ∎

*Remark* 1. We note that estimates of the above type have been used in earlier studies of nonlocal models; see, for example, [20, 46]. We can also reformulate the result of the above lemma as an error estimate of the discrete operators

$$\|(\mathcal{L}_\delta^{-1} - \mathcal{L}_0^{-1})P_N\|_2 = \|P_N(\mathcal{L}_\delta^{-1} - \mathcal{L}_0^{-1})P_N\|_2 \le C\delta^2 \,, \tag{2.17}$$

which can be used to quantify the difference between the spectra of discrete operators.

*Remark* 2. From the standard approximation theory for local models, it is easy to show that $u_N^0$ converges to $u_0$ at least quadratically in $L^2$ if $f$ is bounded in $L^2$. Moreover the convergence can be of exponential order when $f$ or, equivalently, the solution $u_0$, is analytic. By (1.3), we then arrive at

$$\|u_N^\delta - u^0\|_2 \le C\delta^2 + C'N^{-2} \quad \text{or} \quad \|u_N^\delta - u^0\|_2 \le C\delta^2 + C'e^{-cN} \tag{2.18}$$

for some constants $C$, $C'$, and $c$. This leads to (1.2). In particular, it means that Fourier spectral methods are asymptotically compatible for stationary linear nonlocal models. Moreover, we get a uniform error estimate in the sense that the estimates (2.10) and (2.18) hold for any $\delta$ sufficiently small and $N$ sufficiently large, with no restriction on their relative sizes.

COROLLARY 2. *We further have* $\|\mathcal{L}_0^{-2}(\mathcal{L}_\delta - \mathcal{L}_0)f_N\|_2 \le C\delta^2\|f_N\|_2$ *for* $f_N \in \hat{B}_N^o$.

*Proof.* We have proven that $\lambda_0(n) \le \lambda_\delta(n) < 0$ from the previous lemma. This gives $|\lambda_\delta(n)| \le |\lambda_0(n)|$. So,

$$\left|\frac{1}{\lambda_\delta(n)^2}(\lambda_\delta(n) - \lambda_0(n))\right| \le \left|\frac{1}{\lambda_\delta(n)} - \frac{1}{\lambda_0(n)}\right|.$$

This leads to $\|\mathcal{L}_0^{-2}(\mathcal{L}_\delta - \mathcal{L}_0)f_N\|_2 \le \|(\mathcal{L}_\delta^{-1} - \mathcal{L}_0^{-1})f_N\|_2$ for $f_N \in \hat{B}_N^o$. Using (2.17), we get the corollary. ∎

For the next result, we focus on NACs with power law kernels of the form $\rho(\xi) = c_\alpha \xi^{-\alpha}$ for $\xi \in (0,1)$, $\alpha \in (0,3)$, and $c_\alpha = 3 - \alpha$. Then,

$$\rho_\delta(s) = \frac{c_\alpha}{\delta^{3-\alpha}|s|^\alpha} \quad \forall s \in [-\delta, 0) \cup (0, \delta], \quad \alpha \in (0,3). \tag{2.19}$$

Consider the problem (2.5) under periodic boundary conditions; we get a solution

$$u_\delta(x) = a_0^\delta - \sum_{n\neq 0}^{|n|\le\infty} \frac{f_n}{\lambda_\delta(n)} e^{inx}. \tag{2.20}$$

LEMMA 3 (regularity). *If* $f \in H_{per}^s[-\pi,\pi]$, *then* $u_\delta \in H_{per}^{s+\beta}[-\pi,\pi]$ *for* $\alpha \in (0,3)$ *and* $\beta = \max\{0, \alpha - 1\}$.

*Proof.* For $\alpha \in (0,1)$, it is sufficient to prove

$$C_1(\delta) \le |\lambda_\delta(n)| \le C_2(\delta) \quad \forall |n| > 1, \tag{2.21}$$

where $C_1(\delta)$ and $C_2(\delta)$ are positive constants independent of $n$. By (2.3), we get

$$|\lambda_\delta(n)| = \frac{2c_\alpha}{\delta^{3-\alpha}} \int_0^\delta \frac{1 - \cos(ns)}{s^\alpha} ds. \tag{2.22}$$

To obtain the upper bound, by Riemann lemma, we know that

$$\lim_{|n|\to\infty} |\lambda_\delta(n)| = \frac{2c_\alpha}{\delta^{3-\alpha}} \int_0^\delta \frac{1}{s^\alpha} ds \left( \frac{1}{2\pi} \int_0^{2\pi} (1-\cos(s)) ds \right),$$

which is obviously bounded for fixed $\delta$. Now we consider the lower bound. Using the same technique as in (2.15), we have

$$\begin{aligned} |\lambda_\delta(n)| &= \frac{2c_\alpha}{\delta^{3-\alpha}} \left( \int_0^\delta \frac{1}{s^\alpha} ds - \int_0^\delta \frac{\cos(ns)}{s^\alpha} ds \right) \geq \frac{2c_\alpha}{\delta^{3-\alpha}} \left( \int_0^\delta \frac{1}{s^\alpha} ds - \int_0^{\delta_n'} \frac{\cos(ns)}{s^\alpha} ds \right) \\ &\geq \frac{2c_\alpha}{\delta^{3-\alpha}} \left( \int_0^\delta \frac{1}{s^\alpha} ds - \int_0^{\delta_1'} \frac{\cos(s)}{s^\alpha} ds \right) := C_1(\alpha, \delta_1') > 0, \end{aligned}$$

where $\delta_n' = \min\{\delta, \frac{\pi}{2n}\}$. Consequently, we have shown the first case. Now for $\alpha \in (1,3)$, it suffices to show that $C_3(\delta)|n|^{\alpha-1} \leq |\lambda_\delta(n)| \leq C_4(\delta)|n|^{\alpha-1}$ for $|n| > 1$, where $C_2(\delta)$ and $C_3(\delta)$ are positive constants independent of $n$. By (2.22) we have

$$|\lambda_\delta(n)| = \frac{2c_\alpha}{\delta^{3-\alpha}} \int_0^{n\delta} \frac{1-\cos(s)}{s^\alpha} ds |n|^{\alpha-1} := \frac{2c_\alpha}{\delta^{3-\alpha}} Q_n |n|^{\alpha-1}. \tag{2.23}$$

It remains to prove that the positive sequence $\{Q_n\}$ has uniform bounds independent of $n$. For the lower bound, we have for $|n| \geq 1$ and $\delta' = \min\{\delta, 1\}$ that

$$Q_n \geq Q_1 = \int_0^\delta \frac{1-\cos(s)}{s^\alpha} ds \geq \int_0^{\delta'} \left( \frac{1}{2} s^{2-\alpha} - \frac{1}{24} s^{4-\alpha} \right) ds := C_2(\alpha, \delta') > 0. \tag{2.24}$$

For the upper bound, it is equivalent to prove that

$$\lim_{n\to\infty} Q_n = \lim_{n\to\infty} \int_0^{n\delta} \frac{1-\cos(s)}{s^\alpha} ds = \int_0^\infty \frac{1-\cos(s)}{s^\alpha} ds := Q \tag{2.25}$$

is bounded since

$$\begin{aligned} Q &= \int_0^\delta \frac{1-\cos(s)}{s^\alpha} ds + \int_\delta^\infty \frac{1-\cos(s)}{s^\alpha} ds \\ &\leq \int_0^\delta \frac{1}{2} s^{2-\alpha} ds + \int_\delta^\infty \frac{2}{s^\alpha} ds = \frac{\delta^{3-\alpha}}{2(3-\alpha)} + \frac{2}{\alpha-1} \delta^{1-\alpha}. \end{aligned}$$

This completes the proof for the case $\alpha \in (1,3)$. For the special case $\alpha = 1$,

$$|\lambda_\delta(n)| = \frac{4}{\delta^2} \int_0^{\frac{n\delta}{2\pi}} \frac{1-\cos(2\pi\theta)}{\theta} d\theta. \tag{2.26}$$

By (2.24) we get a uniform lower bound for $|\lambda_\delta(n)|$. For large $n$, we can show

$$\int_1^{n+1} \frac{1-\cos(2\pi\theta)}{\theta} d\theta \geq \sum_{k=1}^n \int_{k+\frac{1}{2}}^{k+1} \frac{1-\cos(2\pi\theta)}{\theta} d\theta \geq \frac{1}{2} \sum_{k=1}^n \frac{1}{k+1},$$

$$\int_1^{n+1} \frac{1-\cos(2\pi\theta)}{\theta} d\theta \leq \int_1^{n+1} \frac{2}{\theta} d\theta \leq 2 \sum_{k=1}^n \frac{1}{k}.$$

We see that $|\lambda_\delta(n)|$ are on the order of $\log(n)$ and uniformly bounded below by a positive constant for large $n$. Hence, the lemma remains true for $\alpha = 1$. ∎

Lemma 3 will be used later to characterize steady state solutions of the nonlinear NAC.

**3. Asymptotic compatibility for approximations of NAC.** Consider (1.5) for $x \in (\pi, \pi)$ with a periodic boundary condition and an initial condition $u(0,x) = u_0(x)$; its local limit is the conventional LAC equation

$$\frac{\partial u}{\partial t} = \epsilon^2 \mathcal{L}_0 u + u - u^3. \tag{3.1}$$

Analogously to the local case, we denote the nonlocal free energy by

$$E^\delta(u) = \int_{-\pi}^{\pi} \left( \frac{\epsilon^2}{2} \int_{-\delta}^{\delta} \rho_\delta(s) \frac{(u(x+s) - u(x))^2}{2} ds + \frac{1}{4}(u(x)-1)^2 \right) dx. \tag{3.2}$$

The nonlocal model (1.5) can be viewed as an $L^2$-gradient flow of $E^\delta(u)$ so that

$$\frac{dE^\delta(u^\delta)}{dt} = -\|u_t^\delta\|_2^2. \tag{3.3}$$

It is also natural to consider the so-called conserved dynamics, that is, the nonlocal Cahn–Hilliard equation of the form

$$u_t = \mathcal{L}_\delta(-\epsilon^2 \mathcal{L}_\delta u + u^3 - u), \tag{3.4}$$

which is an analogue of the local Cahn–Hilliard equation and with the $\|u_t^\delta\|_2^2$ term in the energy law replaced by the dual norm of the energy norm associated with $\mathcal{L}_\delta$.

The numerical solutions, given in the form of

$$u_N^\delta(t,x) = \sum_{|n| \le N} a_n^\delta(t) e^{inx}, \quad u_N^0(t,x) = \sum_{|n| \le N} a_n^0(t) e^{inx}, \tag{3.5}$$

are obtained from the approximate schemes

$$\frac{\partial u_N^\delta}{\partial t} = \epsilon^2 \mathcal{L}_\delta u_N^\delta + u_N^\delta - P_N[(u_N^\delta)^3], \tag{3.6}$$

$$\frac{\partial u_N^0}{\partial t} = \epsilon^2 \mathcal{L}_0 u_N^0 + u_N^0 - P_N[(u_N^0)^3]. \tag{3.7}$$

One of the nice properties of NAC and LAC models is the maximum principle. That is, if the initial condition is bounded in magnitude by 1, then the same bound holds at all later times. However, such a pointwise bound of the solutions may not be preserved by the Fourier spectral approximation. This calls for additional numerical stability estimates.

THEOREM 4. *For the solution $u_N^0(t,x)$ to (3.7) given by (3.5), we have*

$$\|u_N^0(t,\cdot)\|_2^2 \le 2\pi, \quad \|u_N^0(t,\cdot)\|_\infty \le C_{L^\infty}(\epsilon, T, u_0) \quad \forall t \in (0,T]. \tag{3.8}$$

*Moreover, we may bound the high-order derivative $\mathcal{L}_0^2 u_N^0$ by*

$$\int_0^T \|\mathcal{L}_0^2 u_N^0(t,\cdot)\|_2 dt \le C_{L^4}(\epsilon, T, u_0). \tag{3.9}$$

*Here $C_{L^\infty}(\epsilon, T, u_0)$ and $C_{L^4}(\epsilon, T, u_0)$ are constants independent of $\delta$ and $N$.*

*Proof.* For (3.8), we refer the reader to [41]. Following standard energy estimates and bootstrap arguments for parabolic equations, we can get (3.9). The details are omitted. ∎

A similar stability result holds for $u_N^\delta$, but it will not be of use in later discussions.

THEOREM 5. *For any finite time $T > 0$, we have*

$$\|u_N^\delta(T,\cdot) - u_N^0(T,\cdot)\|_2 \le C(\epsilon, T, u_0)\delta^2, \tag{3.10}$$

*where $C$ is independent on $\delta$ and $N$.*

*Proof.* First, denote

$$E(t) = \|u_N^\delta(t,\cdot) - u_N^0(t,\cdot)\|_2. \tag{3.11}$$

Simple calculation gives

$$\frac{1}{2}\frac{dE^2}{dt} = \frac{1}{2}\frac{d}{dt}(u_N^\delta - u_N^0, u_N^\delta - u_N^0) = \left(\frac{\partial}{\partial t}u_N^\delta - \frac{\partial}{\partial t}u_N^0, u_N^\delta - u_N^0\right).$$

Substituting (3.6) and (3.7) into the above equation, we get

$$\begin{aligned} E\frac{dE}{dt} &= E^2 + \epsilon^2(\mathcal{L}_\delta u_N^\delta - \mathcal{L}_0 u_N^0, u_N^\delta - u_N^0) - (P_N[(u_N^\delta)^3] - P_N[(u_N^0)^3], u_N^\delta - u_N^0) \\ &:= E^2 + \epsilon^2 \mathrm{I} + \mathrm{II}. \end{aligned}$$

For II, we have $\mathrm{II} = -((u_N^\delta)^3 - (u_N^0)^3, u_N^\delta - u_N^0) \le 0$. Obviously $\|\mathcal{L}_\delta u_N^0\|_2 \le \|\mathcal{L}_0 u_N^0\|_2$. Thus, for I, we have

$$\begin{aligned} \mathrm{I} &= (\mathcal{L}_\delta u_N^\delta - \mathcal{L}_\delta u_N^0 + \mathcal{L}_\delta u_N^0 - \mathcal{L}_0 u_N^0, u_N^\delta - u_N^0) \\ &= (\mathcal{L}_\delta(u_N^\delta - u_N^0), u_N^\delta - u_N^0) + ((\mathcal{L}_\delta - \mathcal{L}_0)u_N^0, u_N^\delta - u_N^0) \le \|(\mathcal{L}_\delta - \mathcal{L}_0)u_N^0\|_2 E, \end{aligned}$$

where the negative definiteness of $\mathcal{L}_\delta$ is used. Since

$$\|(\mathcal{L}_\delta - \mathcal{L}_0)u_N^0\|_2 = \|\mathcal{L}_0^{-2}(\mathcal{L}_\delta - \mathcal{L}_0)\mathcal{L}_0^2 u_N^0\|_2,$$

by Corollary 2, we get $\mathrm{I} \le C\delta^2\|\mathcal{L}_0^2 u_N^0\|_2 E$. Combining these estimates with (3.9), we get

$$\frac{dE}{dt} \le E + C\delta^2\|\mathcal{L}_0^2 u_N^0\|_2.$$

The Gronwall's inequality then leads to the desired result (3.10). ∎

*Remark* 3. In [41], the convergence of Fourier spectral methods for LAC equations was shown. This, once again in combination with Theorem 5, can show that Fourier spectral methods are asymptotically compatible for time-dependent NAC equations according to (1.3) and the discussion given in the introduction. Extensions to other time-dependent nonlinear nonlocal models are also possible.

**4. Numerical simulations and theoretical analysis of nonlocal models.** We now carry out both numerical simulations and theoretical analysis of the nonlocal models, including both linear models and NAC.

**4.1. Implementation of numerical methods.** The implementation of Fourier spectral methods for linear steady state problems is straightforward. For the time-dependent nonlinear NAC (and the local limit, LAC), our task is to compute its Fourier coefficients $\{a_n(t)\}$ in time that satisfy a nonlinear ODE system,

$$\frac{d}{dt}A(t) = (\epsilon^2\Lambda + I)A(t) - H(A(t)),$$

where $I$ is the identity matrix, $A(t) = (a_{-N}, a_{-N+1}, \ldots, a_{-1}, a_0, a_1, \ldots, a_{N-1}, a_N)^T$, and $\Lambda$ has the following forms: the local problem

$$\Lambda = \mathrm{diag}(-N^2, -(N-1)^2, \ldots, -1, 0, -1, \ldots, -(N-1)^2, -N^2)$$

and nonlocal problem

$$\Lambda = \mathrm{diag}(\lambda_\delta(-N), \lambda_\delta(-N+1), \ldots, \lambda_\delta(-1), 0, \lambda_\delta(1), \ldots, \lambda_\delta(N-1), \lambda_\delta(N)),$$

and, finally, the component $H_j$ of the vector $H(A(t))$ can be expressed as

$$H_j = \sum_{|p|,|q|,|r|\le N, p+q+r=j} a_p a_q a_r \quad \text{for} \quad j = -N, -N+1, \ldots, -1, 0, 1, \ldots, N-1, N.$$

To solve the ODE system, we use the standard fourth-order Runge–Kutta method. As for the evaluation of the cubic nonlinear term, if we let

$$M_{jr} = \sum_{|p|,|q|\le N, p+q=j-r} a_p a_q \quad \text{for} \quad j, r = -N, -N+1, \ldots, -1, 0, 1, \ldots, N-1, N,$$

then $H = MA$. It is noted that $M$ is a Toeplitz matrix whose entries can be obtained by fast convolution in $O(N\log(N))$ operations. The cost of evaluating the product of a Toeplitz matrix $M$ with a vector $A$ is also $O(N\log(N))$, as is the total computational cost per time step.

The numerical computation of $\{\lambda_\delta(k)\}$ is another technical aspect of the Fourier spectral discretization. Different methods, using either exact analytical expressions or numerical estimations, can be implemented depending on the specific nonlocal interaction kernel. We discuss a few typical cases here. First, let us consider two kernels that are smooth at the origin:

$$\rho_1(x) \equiv 3 \quad \text{and} \quad \rho_2(x) = 30(x-1)^2. \tag{4.1}$$

Eigenvalues of nonlocal operators associated with kernels $\rho_1$ and $\rho_2$ can be explicitly computed and are given by

$$\lambda_{1,\delta}(n) = \frac{6}{\delta^2}\left(\frac{\sin n\delta}{n\delta} - 1\right),$$

$$\lambda_{2,\delta}(n) = \frac{20}{\delta^2}\left(\frac{6}{n^2\delta^2}\left(1 - \frac{\sin n\delta}{n\delta}\right) - 1\right).$$

We now turn to kernels that are singular at the origin, for example,

$$\rho_\delta(s) = \frac{c_\alpha}{\delta^{3-\alpha}|s|^\alpha} \quad \forall s \in [-\delta, 0) \cup (0, \delta], \quad \alpha \in (0, 3). \tag{4.2}$$

Eigenvalues of the corresponding nonlocal operators are given by the following formulae that do not yield simple analytical expressions:

$$-\lambda_\delta(n) = 2(3-\alpha)\delta^{3-\alpha}|n|^{\alpha-1}\int_0^{n\delta}\frac{1-\cos t}{t^\alpha}dt\,. \tag{4.3}$$

Instead, we compute them numerically. More specifically, let us consider the cases where $\alpha$ equals 0.5, 1, 1.5, or 2. Using integration by parts, we see that the following integrals need to be computed:

$$\text{Fresnel integral:}\quad C(x) = \int_0^x \frac{\cos t}{t^{\frac{1}{2}}}dt \quad \text{for}\ \ \alpha = 0.5,$$

$$\text{Part of cosine integral:}\quad Ci(x) = \gamma + \ln|x| + \int_0^x \frac{\cos t - 1}{t}dt \quad \text{for}\ \ \alpha = 1,$$

$$\text{Fresnel integral:}\quad S(x) = \int_0^x \frac{\sin t}{t^{\frac{1}{2}}}dt \quad \text{for}\ \ \alpha = 1.5,$$

$$\text{Sine integral:}\quad Si(x) = \int_0^x \frac{\sin t}{t}dt \quad \text{for}\ \ \alpha = 2.5.$$

Details on how to effectively and accurately compute these integrals can be found in [11]. As visual illustrations, the eigenvalues are plotted in Figure 2, and the results are consistent with the theory given in Lemma 3.

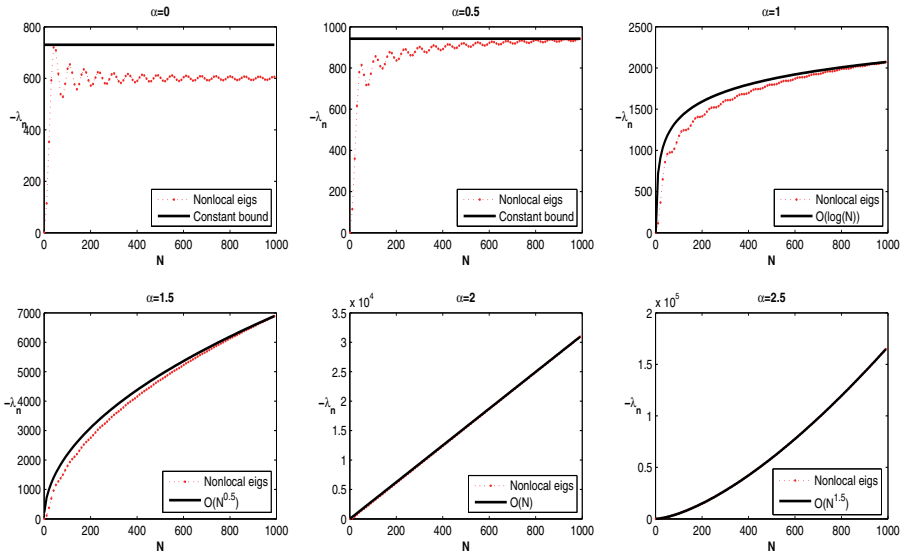


FIG. 2. *Numerical eigenvalues for varying $\alpha$ and a fixed $\delta = 0.1$.*

**4.2. Linear stationary nonlocal problems.** We first report numerical studies of some linear stationary nonlocal problem (2.5) and its local limit problem (2.6).

*Example* 4. We first consider $f(x) = sign(x)$ in $[-\pi, \pi]$ and two smooth kernels in (4.1).

To compare the difference between $u_N^\delta$ and $u_N^0$ numerically, we choose two different numerical resolutions with $N = 100$ or 100000 and vary $\delta$. The results are shown in Table 1. We see that $\|u_N^\delta - u_N^0\|_2$ is indeed second order with respect to $\delta$ uniformly, independent of $N$. This substantiates exactly our theoretical result (2.10).

TABLE 1
*Numerical difference between $u_N^\delta$ and $u_N^0$ with $N_1 = 100$ and $N_2 = 100000$.*

| Kernel | $\delta = 0.1$ | $\|u_{N_1}^\delta - u_{N_1}^0\|_2$ | Rate | $\|u_{N_2}^\delta - u_{N_2}^0\|_2$ | Rate |
|---|---|---|---|---|---|
| $\rho_1$ | $\delta$ | 7.21e-3 | - | 7.08e-3 | - |
| | $\delta/2$ | 1.77e-3 | 2.03 | 1.75e-3 | 2.01 |
| | $\delta/4$ | 4.41e-4 | 2.00 | 4.40e-4 | 1.99 |
| | $\delta/8$ | 1.10e-4 | 2.00 | 1.10e-4 | 2.00 |
| $\rho_2$ | $\delta$ | 3.38e-3 | - | 3.35e-3 | - |
| | $\delta/2$ | 8.41e-4 | 2.01 | 8.37e-4 | 2.00 |
| | $\delta/4$ | 2.10e-4 | 2.00 | 2.09e-4 | 2.00 |
| | $\delta/8$ | 5.47e-5 | 1.94 | 5.45e-5 | 1.94 |

*Example* 5. We now use the same $f$ as above but turn to singular-type kernels given in (4.2). We fix $\delta = 3$ and vary $\alpha$ to be 0.5, 1, 1.5, and 2, respectively.

Before presenting numerical solutions, we make some predictions based on Lemma 3. It is easy to see that the function $f$ has three discontinuous points and is in $H^s$-space for any $s < 1/2$. For $\alpha = 0.5$ and $\alpha = 1$, solutions of nonlocal models have the same regularity class as $f$ with discontinuities being inherited from the source term. When $\alpha > 1$, the solutions are in $H^{s+\alpha-1}$ with $s + \alpha - 1 > 1/2$ and continuous. We also expect that solutions will be getting close to the local limit as $\alpha$ increases.

To provide sufficient numerical resolution, we take $N = 40000$. The numerical solutions for different $\alpha$ are shown in Figure 3 (left). It is seen that there are three obvious jumps at $x = 0, \pm\pi$ in solutions for cases $\alpha = 0.5$ and $\alpha = 1$, but solutions in other cases remain smooth. In Figure 3 (right) we zoom in at $x = 0$ and plot errors between numerical solutions of nonlocal problems and the exact solution to the local problem. We can see more clearly the discontinuities in the solutions with $\alpha = 0.5$ and $\alpha = 1$, but more regular solutions with $\alpha > 1$. Moreover, we also observe that as $\alpha$ increases, the errors decrease. This is consistent with the prediction given in Lemma 3. In addition, Gibbs phenomena occur near the discontinuities in the case $\alpha = 0.5$, which is not surprising, since we use only truncated Fourier series in the approximation.

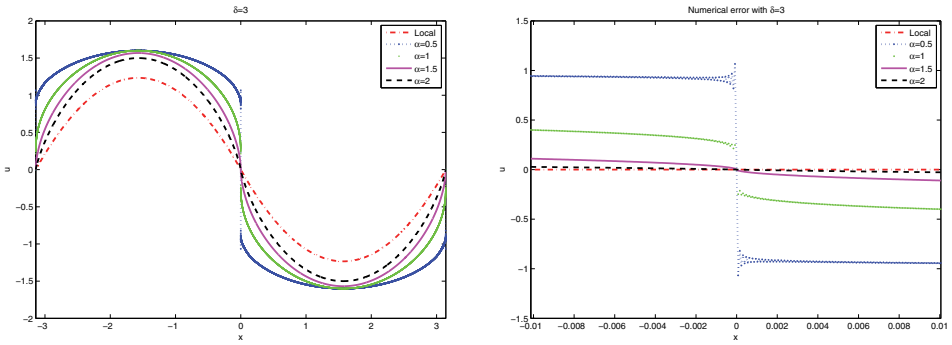


FIG. 3. *Nonlocal solutions for different $\alpha$ and errors with local solution near $x = 0$.*

TABLE 2
*Errors between solutions of NAC and LAC equations.*

| | $T=1$ | | $T=10$ | |
|---|---|---|---|---|
| $\delta = 0.5$ | $\|u_N^\delta - u_N^0\|_2$ | Rate | $\|u_N^\delta - u_N^0\|_2$ | Rate |
| $\delta$ | 9.20e-4 | - | 1.24e-1 | - |
| $\delta/2$ | 2.39e-4 | 1.95 | 2.26e-2 | 2.45 |
| $\delta/4$ | 6.02e-5 | 1.99 | 4.94e-3 | 2.20 |
| $\delta/8$ | 1.51e-5 | 2.00 | 1.20e-3 | 2.04 |

**4.3. Asymptotic compatibility for nonlocal Allen–Cahn equations.** In this part, we aim to show the asymptotic compatibility for NAC equations.

*Example* 6. We consider the 1D NAC equation in $[-\pi, \pi]$ with periodic boundary conditions and the initial value $u_0(x) = 0.05\cos(x) + 0.1\sin(2x) + 0.04\cos(4x)$. We fix $\epsilon = 0.1$ and take the kernel $\rho_2$ defined in (4.1).

We first test numerically the errors between nonlocal and local models. We take large enough $N = 512$ and very small time step $\Delta t = 0.001$ and change $\delta$. Errors at $T = 1$ and $T = 10$ are shown in Table 2. It is seen that the convergence rate is about $O(\delta^2)$, as predicted by theoretical results.

We next investigate the dynamics of the time-dependent equations. We choose a set of particular values for the discretization parameters. The time step in RK4 methods is taken as $\Delta t = 0.01$. For the local model, we take $N = 128$, but take $N = 4096$ for the nonlocal model. Both cases, with a big delta $\delta = 3$ and a small $\delta = 0.3$, are used to compare with the local solutions.

In Figure 4, we observe that solutions of nonlocal models are close to the local ones for small $\delta$, but there are much greater differences in the local ones for large $\delta$. Again, jumps appearing in the nonlocal solutions are very obvious with large $\delta$ but less evident in solutions of the local model and nonlocal models with small $\delta$.

**4.4. Steady states of nonlocal Allen–Cahn equations.** It is well known that steady states of Allen–Cahn equations with a finite $\epsilon$ are infinitely smooth. This, however, is not true for NAC. Let us consider the solution of

$$\epsilon^2 \mathcal{L}_\delta u^* + u^* - u^{*3} = 0, \tag{4.4}$$

with kernels given by (2.19) and periodic boundary conditions. We only consider solutions with finite energy, so that they are necessarily bounded pointwise.

*Case* I: $0 \le \alpha < 1$. We have an integrable kernel and denote

$$C_\delta := \int_{-\delta}^{\delta} \rho_\delta(s) ds = \frac{2(3-\alpha)}{1-\alpha}\delta^{-2}. \tag{4.5}$$

It turns out the parameter $\epsilon^2 C_\delta = 1$ is a critical value as demonstrated from our experiments and analysis. We emphasize that the following results hold for other kinds of integrable kernels but perhaps with different parameters and critical values. First, our numerical experiments, reported later, show that we get continuous solutions to (4.4) if $\epsilon^2 C_\delta \ge 1$. This can be rigorously confirmed as follows.

PROPOSITION 6. *If $\epsilon^2 C_\delta \ge 1$, then the solution $u^*$ is continuous.*

*Proof.* Since the kernel is integrable, we have

$$\mathcal{L}_\delta u^*(x) = \int_{-\delta}^{\delta} \rho_\delta(s) u^*(x+s) ds - u^*(x) \int_{-\delta}^{\delta} \rho_\delta(s) ds := I(x) - C_\delta u^*(x),$$

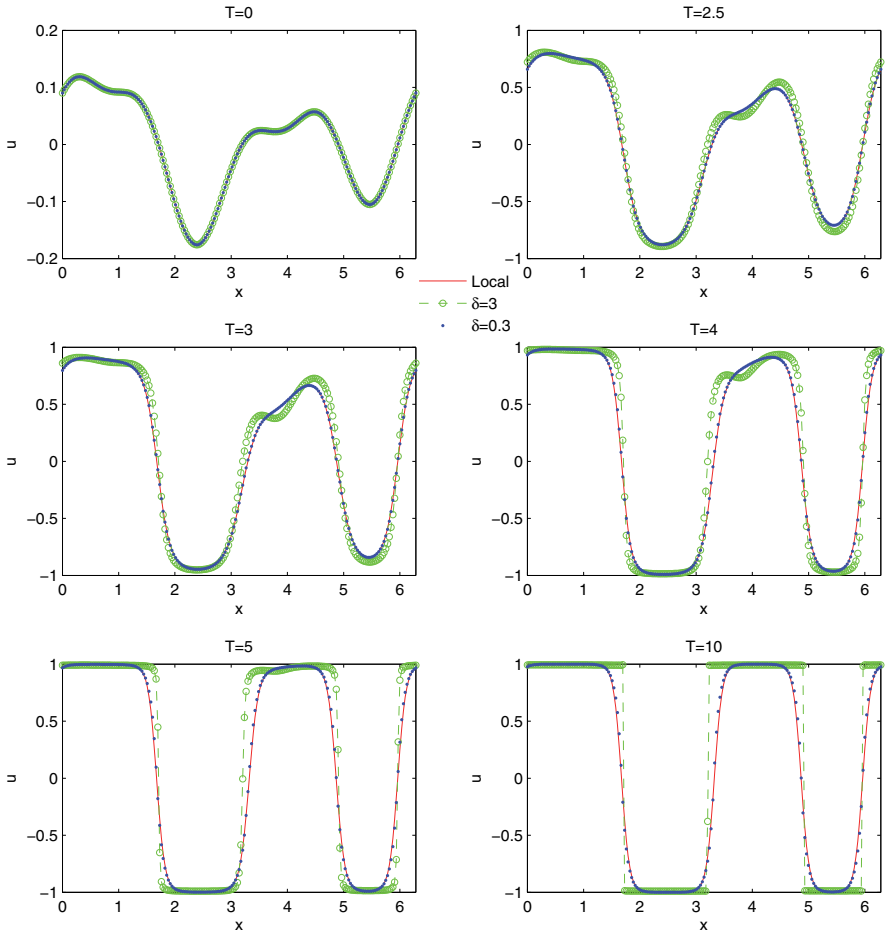


FIG. 4. *Numerical evolutions of both LAC and NAC equations.*

where $I(x)$ is the convolution of two integrable functions and thus continuous. Moreover, (4.4) is equivalent to

$$\epsilon^2 I(x) = (\epsilon^2 C_\delta - 1)u^*(x) + u^*(x)^3 \quad \forall x\,. \tag{4.6}$$

For $\epsilon^2 C_\delta - 1 \geq 0$, the right-hand side is a strictly increasing continuous function of $u$, and thus it has a continuous inverse. The continuity of $u$ then follows from that of $I(x)$. ∎

If $\epsilon^2 C_\delta < 1$, there is ample numerical evidence for the appearance of discontinuities at isolated interface points, namely where $u^*$ vanish. More specifically, assume that $u^*$ has an isolated interface point $x_*$ that is at least $2\delta$ away from other interfaces and within the $\delta$ neighborhood, and that $u^*$ is monotonic (increasing, without loss of generality). Then the discontinuities across interfaces can be justified.

PROPOSITION 7. *With the above assumptions, if $\epsilon^2 C_\delta < 1$, the locally increasing $u^*$ has a discontinuity at $x_*$. Moreover,*

$$\lim_{x \to x_*^+} u^*(x) = \sqrt{1 - \epsilon^2 C_\delta}, \qquad \lim_{x \to x_*^-} u^*(x) = -\sqrt{1 - \epsilon^2 C_\delta}. \tag{4.7}$$

*Proof.* Note that $u^*(x) > 0\ \forall x \in (x_*, x_* + 2\delta)$ and $u^*(x) < 0\ \forall x \in (x_* - 2\delta, x_*)$. By (4.6) we have $I(x_*) = 0$ since $u^*(x_*) = 0$. For any $x \in (x_*, x_* + \delta)$, due to the monotonicity assumption, $u^*(x + s) \geq u^*(x_* + s)$, for any $s \in (-\delta, \delta)$, so

$$I(x) = I(x) - I(x_*) = \int_{-\delta}^{\delta} \rho_\delta(s)(u^*(x + s) - u^*(x_* + s))ds \geq 0.$$

Equation (4.6) then implies $u^*(x)^2 \geq 1 - \epsilon^2 C_\delta\ \forall x \in (x_*, x_* + \delta)$. This shows that $u^*$ cannot be continuous at $x_*$. Moreover, from the above argument, we see that the inequalities (4.7) hold as $\lim_{x \to x_*} I(x) = 0$. ∎

*Case* II: $1 \leq \alpha \leq 3/2$. This case is open. We speculate that there is discontinuity for case $\alpha = 1$ but not for the case $\alpha = 1.5$, but our numerical results are inconclusive.

*Case* III: $3/2 < \alpha < 3$. By (4.4) and the maximum principle, we may apply Lemma 3 to get $u^* \in H^{\alpha-1}$. As $s - 1 > 1/2$, by the embedding theorem in one dimension, we know $u^*(x)$ is continuous.

*Case* IV: $2 \leq \alpha < 3$. Here, by Lemma 3 we may actually get $u^*(x) \in H^{\alpha-1} \subset H^1$. This further leads to $u^* \in H^{1+\alpha-1} \subset H^2$ again by Lemma 3. With a bootstrapping argument, we can see that $u^*$ is infinitely smooth.

*Numerical evidence.* We numerically search for the steady state solutions through a gradient flow. We shift the interval to $(0, 2\pi)$ and start with an initial state $u_0(x) = 0.05\cos(x)$. Numerical evidence suggests that an interface in the steady state solution is located at $x = \pi$ (the center of the interval).

*Example* 7. We first look at the case with a kernel of the form (2.19) for $\alpha = 0.5$. By (4.7), the theoretically predicted jump is $\sqrt{1 - 10\epsilon^2/\delta^2}$. The numerically computed jumps with varying $\epsilon$ and $\delta$ are given in Table 3. We observe that the numerical jumps are very close to the theoretical ones.

TABLE 3
*Numerical jumps and theoretical jumps for NAC equations.*

| | $\epsilon = 0.1$ | | | $\delta = 0.5$ | | |
|---|---|---|---|---|---|---|
| | $\delta = 0.2$ | $\delta = 0.4$ | $\delta = 0.8$ | $\epsilon = 0.05$ | $\epsilon = 0.1$ | $\epsilon = 0.2$ |
| Theoretical | 0 | 0.612 | 0.919 | 0.949 | 0.775 | 0 |
| Numerical | 0 | 0.591 | 0.859 | 0.887 | 0.731 | 0 |

For this example, we perform three groups of simulations. In each case, we change one parameter among $\epsilon$, $\delta$, and $\alpha$, with the other two being fixed. To verify the continuity or discontinuity of steady states, we compute the semi-$H^{\frac{1}{2}}$ norm given by

$$|u_N(\cdot)|_{H^{\frac{1}{2}}} = \left( \sum_{|n| \leq N} |n|\, |u_n|^2 \right)^{\frac{1}{2}}.$$

First, we keep $\epsilon = 0.1$ and $\alpha = 0.5$, and take $\delta$ as 0.2, 0.4 and 0.8. Numerical results are presented in Figure 5. The evolution of the semi-$H^{\frac{1}{2}}$ norm in the left bottom corner indicates that the solution indeed reaches steady state within the interval of simulation. Both by the graphs of solutions around the interface in the right upper corner and by the behavior of semi-$H^{\frac{1}{2}}$ norms with increasing frequency number $N$ in the right bottom corner, we can claim that only when $\delta = 0.2$ is the steady state continuous. There are discontinuities around the interface for the other two cases.

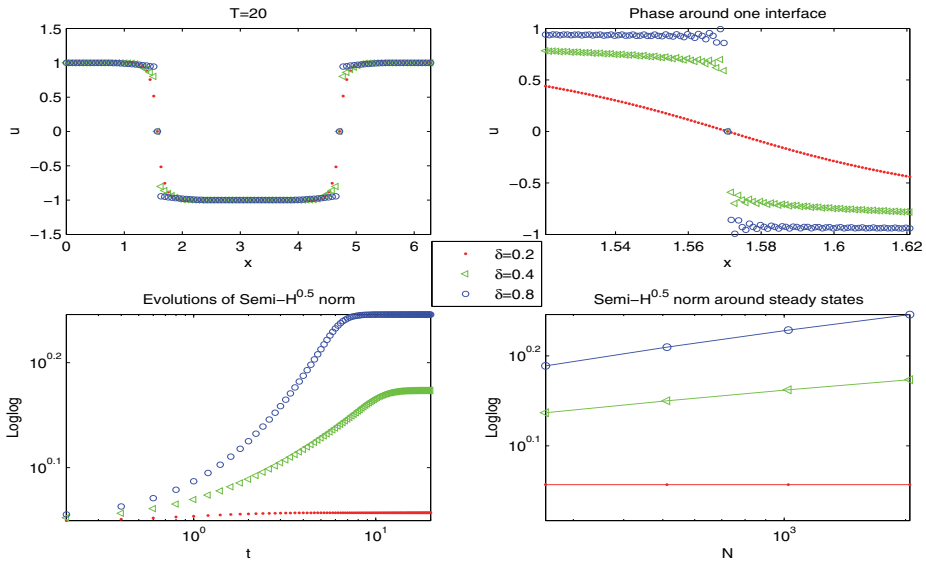


FIG. 5. *Keeping* $\epsilon = 0.1$ *and* $\alpha = 0.5$ *and taking* $\delta$ *as* 0.2, 0.4, *and* 0.8 *in NAC equations.*

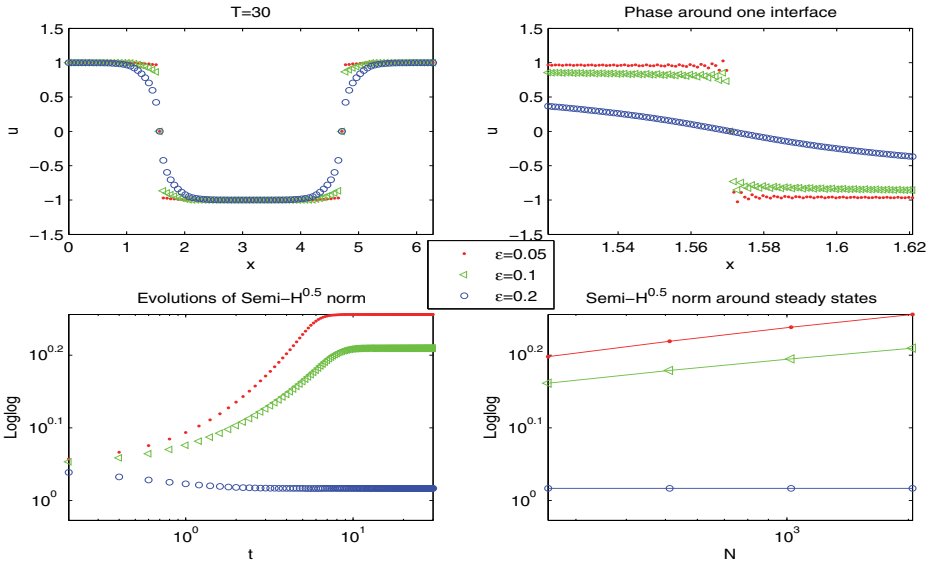


FIG. 6. *Keeping* $\delta = 0.5$ *and* $\alpha = 0.5$ *and taking* $\epsilon$ *as* 0.05, 0.1, *and* 0.2 *in NAC equations.*

Meanwhile, we can check that the condition in Proposition 6 is satisfied only for the case $\delta = 0.2$.

In Figure 6, $\epsilon$ is chosen as 0.05, 0.1, and 0.2, and we fix $\delta = 0.5$ and $\alpha = 0.5$. Similar phenomena can be observed as in the previous set of experiments. Only when the condition in Proposition 6 is satisfied is the steady state continuous. Otherwise, the jump can be quantified by (4.7) as in Proposition 7.

In the final set of simulations, we choose the $\alpha$ as 1, 1.5, 2, and 2.5 and keep $\epsilon$ and $\delta$ fixed. From the behavior of numerical solutions around the interface and the semi-

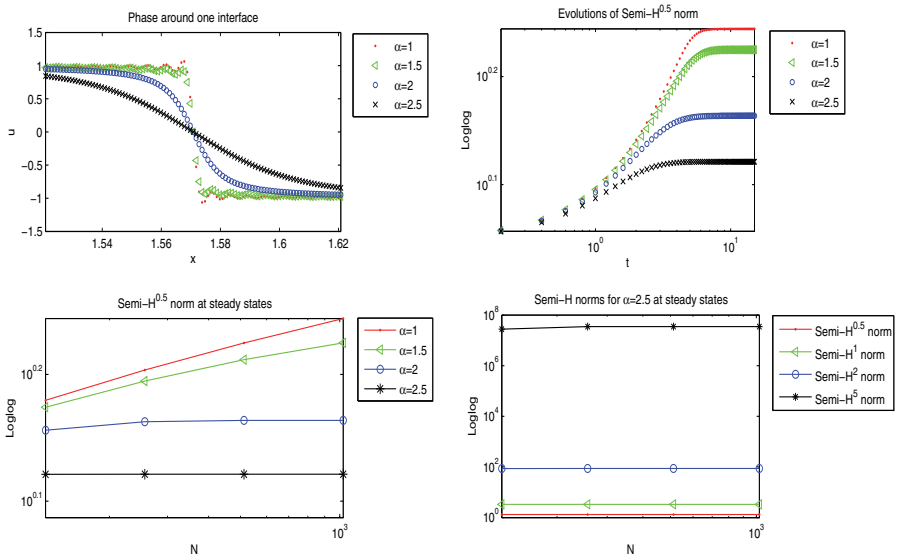


FIG. 7. *Keeping* $\epsilon = 0.1$ *and* $\delta = 1$ *and taking* $\alpha$ *as* $1, 1,5, 2,$ *and* $2.5$ *in NAC equations.*

$H^{\frac{1}{2}}$ norm shown in Figure 7, we can speculate that the steady state is discontinuous for $\alpha = 1$, while theoretically there is no prediction made in this case. For $\alpha = 1.5$, it is hard to tell whether the steady state is continuous or not, since the semi-$H^{\frac{1}{2}}$ norm appears to be convergent as $N$ increases, so we have an inconclusive situation. For $\alpha = 2$ and $\alpha = 2.5$, both analysis and simulations show that steady states are continuous and, in particular, the one corresponding to $\alpha = 2.5$ appears to be very smooth.

In summary, the reports of numerical results are consistent with the established theory. Moreover, they offer some interesting predictions and speculations on the dynamics and steady states of NAC.

**5. Concluding remarks.** This work contains some studies on the Fourier spectral approximations of nonlocal models. While there have been various studies in the literature both on the nonlocal models and their numerical approximations, including ones based on the spectral methods, our contribution lies in the careful examination of approximation properties of the Fourier spectral methods for both nonlocal models and their local limits.

The theme of our study is naturally related to that initiated in [42] on asymptotically compatible schemes. The framework given in [43] is very general and can be applied to different discretizations, but the examples used to illustrate the theory have largely been limited to finite element and finite difference schemes. Here, we successfully established that the numerical solutions of nonlocal models uniformly converge to the corresponding local models with respect to the horizon parameter. More specifically, the difference between the approximations to nonlocal models and their local limit is uniform with respect to the number of Fourier modes and is of $O(\delta^2)$ order, which matches the order of the difference between the exact solutions. This uniform convergence, together with known convergence of Fourier spectral methods for local models, helps to verify the asymptotic compatibility of Fourier spectral methods for nonlocal models without extra assumptions on the solution regularity. In addition,

the rigorously derived asymptotic error estimates (for smooth local solutions) are also new in the literature. Their discovery was possible because of the readily available information on the spectra of particular nonlocal operators under consideration when periodic boundary conditions are imposed. Moreover, we studied steady states of NAC models with different kernels and a finite horizon parameter via both numerical simulations and theoretical analysis and demonstrated the effectiveness of nonlocal models in handling solution singularities.

While our study is focused on NAC models, it is natural to ask whether the theory can be applied to the conservative nonlocal Cahn–Hilliard model. The essential difficulty for the latter is the lack of maximum norm estimates on discrete solutions for general kernels and particularly integrable kernels. This makes it difficult to estimate the Lipschitz constant on the nonlinear term. There are two possible remedies, one being the use of kernels with certain fractional powers so as to invoke embedding of fractional spaces to $L^\infty$, and the other being the replacement of the cubic nonlinear term by a globally Lipschitz term. In terms of time discretization, we briefly mention that the theoretical analysis can be extended to fully discrete schemes. In particular, for the implicit Euler scheme and the standard Crank–Nicolson scheme, it is possible to show that these two fully discrete schemes still preserve the asymptotic compatibility with uniform error estimates.

Finally, singular solutions to nonlocal models pose new challenges to numerical discretizations. While spectral methods are shown to preserve many good properties, such as asymptotic compatibility, and are able to capture the discontinuities in solutions, the spurious Gibbs phenomena do appear. Given recent developments in the context of spectral methods for PDEs on effective singularity detection algorithms and high-order recovery of solution information near and away from singularities [40], it is natural to pursue further studies on how to apply and extend those techniques to nonlocal models.

## REFERENCES


[1] B. Aksoylu and M. L. Parks, *Variational theory and domain decomposition for nonlocal problems*, Appl. Math. Comput., 217 (2011), pp. 6498–6515.

[2] S. M. Allen and J. W. Cahn, *A microscopic theory for antiphase boundary motion and its application to antiphase domain coarsening*, Acta Metall., 27 (1979), pp. 1085–1095.

[3] F. Andreu, J. M. Mazon, J. D. Rossi, and J. Toledo, *Nonlocal Diffusion Problems*, Math. Surveys Monographs 165, AMS, Providence, RI, 2010.

[4] D. Applebaum, *Levy Processes and Stochastic Calculus*, Cambridge Stud. Adv. Math. 93, Cambridge University Press, Cambridge, UK, 2004.

[5] E. Askari, F. Bobaru, R. B. Lehoucq, M. L. Parks, S. A. Silling, and O. Weckner, *Peridynamics for multiscale materials modeling*, J. Phys. Conf. Ser., 125 (2008), pp. 12–78.

[6] P. W. Bates and A. Chmaj, *An integrodifferential model for phase transitions: Stationary solutions in higher space dimensions*, J. Statist. Phys., 95 (1999), pp. 1119–1139.

[7] F. Bobaru and M. Duangpanya, *The peridynamic formulation for transient heat conduction*, Internat. J. Heat Mass Transfer, 53 (2010), pp. 4047–4059.

[8] F. Bobaru, M. Yang, L. F. Alves, S. A. Silling, E. Askari, and J. Xu, *Convergence, adaptive refinement, and scaling in* 1*d peridynamics*, Internat. J. Numer. Methods Engrg., 77 (2009), pp. 852–877.

[9] A. Buades, B. Coll, and J. M. Morel, *Image denoising methods. A new nonlocal principle*, SIAM Rev., 52 (2010), pp. 113–147, doi:10.1137/090773908.

[10] A. Bueno-Orovio, D. Kay, and K. Burrage, *Fourier spectral methods for fractional-in-space reaction-diffusion equations*, BIT, 54 (2014), pp. 937–954.

[11] R. Bulirsch, *Handbook series special functions: Numerical calculation of the sine, cosine and fresnel integrals,* Numer. Math., 9 (1967), pp. 380–385.

[12] N. Burch and R. B. Lehoucq, *Classical, nonlocal, and fractional diffusion equations on bounded domains*, Internat. J. Multiscale Comput. Engrg., 9 (2011), pp. 661–674.

[13] L. Q. Chen and J. Shen, *Applications of semi-implicit Fourier-spectral method to phase field equations*, Comput. Phys. Commun., 108 (1998), pp. 147–158.
[14] X. Chen and M. Gunzburger, *Continuous and discontinuous finite element methods for a peridynamics model of mechanics*, Comput. Methods Appl. Mech. Engrg., 200 (2011), pp. 1237–1250.
[15] A. Chmaj and X. F. Ren, *Homoclinic solutions of an integral equation: Existence and stability*, J. Differential Equations, 155 (1999), pp. 17–43.
[16] Q. Du, M. Gunzburger, R. B. Lehoucq, and K. Zhou, *Analysis and approximation of nonlocal diffusion problems with volume constraints*, SIAM Rev., 54 (2012), pp. 676–696, doi:10.1137/110833294.
[17] Q. Du, M. Gunzburger, R. B. Lehoucq, and K. Zhou, *A nonlocal vector calculus, nonlocal volume-constrained problems, and nonlocal balance laws*, Math. Models Methods Appl. Sci., 23 (2013), pp. 493–540.
[18] Q. Du, L. Ju, L. Tian, and K. Zhou, *A posteriori error analysis of finite element method for linear nonlocal diffusion and peridynamic models*, Math. Comp., 82 (2013), pp. 1889–1922.
[19] Q. Du and R. A. Nicolaides, *Numerical analysis of a continuum model of phase transition*, SIAM J. Numer. Anal., 28 (1991), pp. 1310–1322, doi:10.1137/0728069.
[20] Q. Du and K. Zhou, *Mathematical analysis for the peridynamic nonlocal continuum theory*, Math. Model. Numer. Anal., 45 (2011), pp. 217–234.
[21] X. B. Feng and A. Prohl, *Numerical analysis of the Allen-Cahn equation and approximation for mean curvature flows*, Numer. Math., 94 (2003), pp. 33–65.
[22] P. Fife, *Some nonclassical trends in parabolic and parabolic-like evolutions*, in Trends in Nonlinear Analysis, Springer, Berlin, 2003, pp. 153–191.
[23] G. Gilboa and S. Osher, *Nonlocal operators with applications to image processing*, Multiscale Model. Simul., 7 (2008), pp. 1005–1028, doi:10.1137/070698592.
[24] Z. Guan, J. Lowengrub, C. Wang, and S. Wise, *Second order convex splitting schemes for periodic nonlocal Cahn–Hilliard and Allen–Cahn equations*, J. Comput. Phys., 277 (2014), pp. 48–71.
[25] C. Gui and M. Zhao, *Traveling wave solutions of Allen–Cahn equation with a fractional Laplacian*, Ann. Inst. H. Poincaré Anal. Non Linéaire, 32 (2015), pp. 785–812.
[26] L. D. Landau and E. M. Lifshitz, *Statistical Physics, Part* I, Pergamon Press, Oxford, 1980.
[27] J.-G. Liu and L. Mieussens, *Analysis of an asymptotic preserving scheme for linear kinetic equations in the diffusion limit*, SIAM J. Numer. Anal., 48 (2010), pp. 1474–1491, doi:10.1137/090772770.
[28] Y. Lou, X. Zhang, S. Osher, and A. Bertozzi, *Image recovery via nonlocal operators*, J. Sci. Comput., 42 (2010), pp. 185–197.
[29] R. Macek and S. A. Silling, *Peridynamics via finite element analysis*, Finite Elements Anal. Design, 43 (2007), pp. 1169–1178.
[30] E. Oterkus and E. Madenci, *Peridynamic analysis of fiber-reinforced composite materials*, J. Mech. Materials Structures, 7 (2013), pp. 45–84.
[31] G. Palatucci, O. Savin, and E. Valdinoci, *Local and global minimizers for a variational energy involving a fractional norm*, Ann. Mat. Pura Appl. (4), 192 (2013), pp. 673–718.
[32] L. M. Pismen, *Nonlocal diffuse interface theory of thin films and the moving contact line*, Phys. Rev. E, 64 (2001), 021603.
[33] J. Rowlinson, *Translation of J. D. van der Waals "The thermodynamic theory of capillarity under the hypothesis of a continuous variation of density,"* J. Statist. Phys., 20 (1979), pp. 200–244.
[34] P. Seleson, M. L. Parks, M. Gunzburger, and R. B. Lehoucq, *Peridynamics as an upscaling of molecular dynamics*, Multiscale Model. Simul., 8 (2009), pp. 204–227, doi:10.1137/09074807X.
[35] J. Shen and T. Tang, *Spectral and High-Order Methods with Applications*, Math. Monogr. Ser. 3, Science Press, Beijing, 2006.
[36] S. A. Silling, *Reformulation of elasticity theory for discontinuities and long-range forces*, J. Mech. Phys. Solids, 48 (2000), pp. 175–209.
[37] S. A. Silling and E. Askari, *A meshfree method based on the peridynamic model of solid mechanics*, Comput. Structures, 83 (2005), pp. 1526–1535.
[38] S. A. Silling and R. B. Lehoucq, *Peridynamic theory of solid mechanics*, Adv. Appl. Mech., 44 (2010), pp. 73–168.
[39] S. A. Silling, O. Weckner, E. Askari, and F. Bobaru, *Crack nucleation in a peridynamic solid*, Internat. J. Fracture, 162 (2010), pp. 219–227.
[40] E. Tadmor, *Filters, mollifiers and the computation of the Gibbs phenomenon*, Acta Numer., 16 (2007), pp. 305–378.

[41] T. Tang and J. Yang, *Analysis on Fourier Spectral Methods for Allen-Cahn Equations*, preprint, Hong Kong Baptist University, 2014.

[42] X. Tian and Q. Du, *Analysis and comparison of different approximations to nonlocal diffusion and linear peridynamic equations*, SIAM J. Numer. Anal., 51 (2013), pp. 3458–3482, doi:10.1137/13091631X.

[43] X. Tian and Q. Du, *Asymptotically compatible schemes and applications to robust discretization of nonlocal models*, SIAM J. Numer. Anal., 52 (2014), pp. 1641–1665, doi:10.1137/130942644.

[44] H. Wang and H. Tian, *A fast Galerkin method with efficient matrix assembly and storage for a peridynamic model*, J. Comput. Phys., 240 (2012), pp. 49–57.

[45] J. Zhang and Q. Du, *Numerical studies of discrete approximations to the Allen–Cahn equation in the sharp interface limit*, SIAM J. Sci. Comput., 31 (2009), pp. 3042–3063, doi:10.1137/080738398.

[46] K. Zhou and Q. Du, *Mathematical and numerical analysis of linear peridynamic models with nonlocal boundary conditions*, SIAM J. Numer. Anal., 48 (2010), pp. 1759–1780, doi:10.1137/090781267.